

A late Holocene record of marine high-energy events along the Atlantic coast of Morocco: new evidences from the Tahaddart estuary

Otmane Khalfaoui, Laurent Dezileau, Jean-Philippe Degeai, Maria Snoussi

▶ **To cite this version:**

Otmane Khalfaoui, Laurent Dezileau, Jean-Philippe Degeai, Maria Snoussi. A late Holocene record of marine high-energy events along the Atlantic coast of Morocco: new evidences from the Tahaddart estuary. Geoenvironmental Disasters, 2020, 7 (1), pp.31. 10.1186/s40677-020-00169-5 . hal-03959166

HAL Id: hal-03959166

https://normandie-univ.hal.science/hal-03959166

Submitted on 28 Jan 2023

HAL is a multi-disciplinary open access archive for the deposit and dissemination of scientific research documents, whether they are published or not. The documents may come from teaching and research institutions in France or abroad, or from public or private research centers.

L'archive ouverte pluridisciplinaire **HAL**, est destinée au dépôt et à la diffusion de documents scientifiques de niveau recherche, publiés ou non, émanant des établissements d'enseignement et de recherche français ou étrangers, des laboratoires publics ou privés.



Distributed under a Creative Commons Attribution 4.0 International License

Geoenvironmental Disasters

RESEARCH Open Access

A late Holocene record of marine high-energy events along the Atlantic coast of Morocco: new evidences from the Tahaddart estuary

Otmane Khalfaoui[1,2*], Laurent Dezileau[1*], Jean-Philippe Degeai[3] and Maria Snoussi[2]

Abstract

The Atlantic coast of Morocco has been exposed to marine submersion events from storm surges and tsunamis which have resulted in human and economic losses. The absence of long term records for these hazards makes it difficult to trace their behavior through time, which is the first step to prepare proactive adaptation strategies for events that may happen in the future. In this paper, we present a late Holocene record of marine submersion events along the Atlantic coast of Morocco using a 2.7 m sediment core sampled from the Tahaddart estuary. The sedimentological and geochemical analyses conducted on this geological archive showed a mud-dominated sequence with 14 allochthonous sandy layers (E1-E14) left by marine high-energy events. The deposition age of three layers (E1, E13 and E14) has been determined using conventional dating methods ($^{210}Pb_{ex}$, ^{137}Cs and ^{14}C). The first layer, introduced as E1 seems to fit with the great Lisbon tsunami in 1755 CE (Common Era), an event dated for the first time along the Atlantic coast of Morocco. The other two layers, referred to as E13 and E14, were dated between 3464 and 2837 cal BP (calibrated years Before Present) and chronologically correlated with marine high-energy deposits found on the Spanish Atlantic coast. This correlation confirms the existence of another regional event around 3200 BP.

Keywords: Storm surges, Tsunamis, Late Holocene, Atlantic coast of Morocco, Tahaddart estuary

Introduction

The Atlantic coast of Morocco is already suffering from diverse human pressures, including urban sprawl, pollution and the over-exploitation of coastal resources (Snoussi et al. 2008). Marine high-energy events are putting additional pressure on this area, causing temporary flooding of coastal lowlands and placing life and property at risk. A primary example is tsunami waves, which have historically been reported multiple times along Morocco's Atlantic coast. The most devastating one recorded is the tsunami of Lisbon in 1755 CE (Blanc 2009). During this event, property damage and loss of life were reported in several cities between Tangier and Agadir (Mellas 2012). Two main sources are believed to have triggered these historical tsunamic events: (1) a seismic source related to the tectonic activities in the Gulf of Cadiz, as a result of the convergence between the Eurasian and African plates. Indeed, several earthquakes are regularly generated in this area, some of which have been able to produce tsunami waves (El Alami and Tinti 1991; Gutscher et al. 2006); (2) a volcanic source that has been highly publicized, is the Cumbre Vieja volcano, located in the Canary Islands. A large eruption from this volcano could cause a flank slide, leading to a large amplitude tsunami (Ward and Day 2001; Abadie et al. 2012). Other prevalent events

* Correspondence: m.otmanekhalfaoui@gmail.com; laurent.dezileau@unicaen.fr
[1]Normandie Univ, UNICAEN, UNIROUEN, CNRS, M2C, 14000 Caen, France
Full list of author information is available at the end of the article

Springer Open

© The Author(s). 2020 **Open Access** This article is licensed under a Creative Commons Attribution 4.0 International License, which permits use, sharing, adaptation, distribution and reproduction in any medium or format, as long as you give appropriate credit to the original author(s) and the source, provide a link to the Creative Commons licence, and indicate if changes were made. The images or other third party material in this article are included in the article's Creative Commons licence, unless indicated otherwise in a credit line to the material. If material is not included in the article's Creative Commons licence and your intended use is not permitted by statutory regulation or exceeds the permitted use, you will need to obtain permission directly from the copyright holder. To view a copy of this licence, visit http://creativecommons.org/licenses/by/4.0/.

are winter storms, which are more frequent than tsunamis. They are generated through North Atlantic depressions, or by sporadic cyclones such as Vince (8–11 October 2005) and Leslie (11–14 October 2018) (El Messaoudi et al. 2016; Mhammdi et al. 2020). The storm on 7 January 2014 (also called Hercules/Christina) was very violent, with a maximum wave height of 13.6 m recorded by the Mohammedia buoy (Mhammdi et al. 2020).

Studies on past and present marine submersions are now obvious for countries threatened by these coastal hazards, especially in a context of population growth and coastal development (Degeai et al. 2015). The current state of knowledge on these events along the Atlantic coast of Morocco is based mainly on sparse textual and instrumental records, which is insufficient to understand the behavior of these low-frequency, high-impact events (Raji et al. 2015). During the last 10 years, there has been a growing interest in geological archives along this coast in an effort to overcome this issue. As a result, geological traces of these marine incursions have been recognized at several coastal sites (Fig. 1). They are represented in the form of (1) mega-blocks, also known as boulderite deposits, spread over the beaches of Larache (Mhammdi et al. 2015), Rabat-Skhirat (Mhammdi et al. 2008; Medina et al. 2011), Sidi Moussa (Mellas 2012) and Safi (Theilen-Willige et al. 2013), (2) or as fine sediment (typically sand size) over the coast of Rabat-Skhiratte and Tahaddart (Chahid et al. 2016; El Talibi et al. 2016), the lagoons of Oualidia-Sidi Moussa (Leorri et al. 2010; Mellas 2012) and the Loukous estuary (Mhammdi et al. 2015). Despite these efforts, the majority of these sedimentary deposits lack chronological data, which makes it difficult to know the events responsible for their establishment. Thus, identifying their chronological correlation with other deposits on a local and regional scale becomes an impossible task. Through this study, we present new geological traces of marine submersion events on the Moroccan Atlantic coast, using a sedimentary core collected from the Tahaddart estuary (southwestern coast of Tangier). The results presented are based on a multi-proxy approach that combines sedimentological and geochemical analyses, supported by chronological data (^{137}Cs, $^{210}Pb_{ex}$ and ^{14}C). Furthermore, an attempt to chronologically connect these deposits with historical records of marine high-energy events is presented at the end of this paper.

Research area

The Tahaddart estuary is located in the northern part of the Moroccan Atlantic coast between the two cities of Tanger and Asilah (coordinates: 35°30′ - 35°40′ latitudes North and 5°55′-6°01′ longitudes West). It is the widest and most important marshland along the Tangier Peninsula with an area of 140 km^2.

The climate of the region is Mediterranean with an Atlantic influence, characterized by a wet winter and a hot, dry summer (El Gharbaoui 1981). The estuary is exposed to both westerly winds, called “Rharbi”, from December to April, and easterly winds, called “Chergui” from March to November (Jaaidi et al. 1993). The strongest swells are above 4 m, and the weakest are around 1 m. Most of these swells come from the West to North-West sector, with a dominance of the WNW direction, responsible for the longshore drift (Taaouati 2012). The area is mesotidal, changing between 1 and 3 m, with a semi-diurnal periodicity (ONE 2002). Its influence can be felt up to 13 km from the mouth of the Tahaddart River.

The Tahaddart River drains a catchment area of nearly 1200 km^2 with an average flow rate of 2.3 m^3/s (ONE 2002). It is formed by two main entities separated by the Haouta Beni Mediar hill formation: The M’Harhar River in the northern part, interrupted by the “Ibn Battota” dam, and the Hachef River in the southern part, dammed by the 09 April 1947 dam. These two rivers meet 4 km from the coast to form the Tahaddart River (Fig. 1). The watershed is located on the NW part of the Rif chain; it is composed of Numidian sandstones, marls and limestone-marls deposits of Meso-Cenozoic age (Durand-Delga and Kornprobst 1985). The ensemble is covered by Quaternary river sediments. On the coast, the estuary is protected from high-energy dynamics of the open sea with beach and coastal dune systems up to 7 m, topped to the east by low hills partly covered with forest or pre-forest vegetation (e.g. Charf Akab forest; Boughaba 1992).

The main human impact in the Tahaddart estuary is the construction of the Tangier highway and the thermal power station (Fig. 1). The few villages in the area have a total population of about 45,043 and their inhabitants are living mostly on agriculture, fishing and sea salt production (RGPH 2014). In spite of these anthropic pressures, the Tahaddart estuary has preserved, almost entirely, its natural aspects, which is recommended when searching for past marine submersion deposits (Keating et al. 2008; Aitali et al. 2020). Since 1996, the area was classified by the Moroccan government as a Site of Biological and Ecological Interest (SIBE L11), and in 2005 as a RAMS AR zone under the name of “Complexe du bas Tahaddart” (Nachite et al. 2008).

Sampling and analytical methods

Sample collection

A sedimentary core of 2.7 m in length and 5 cm in diameter (TAH17–1) was collected from the

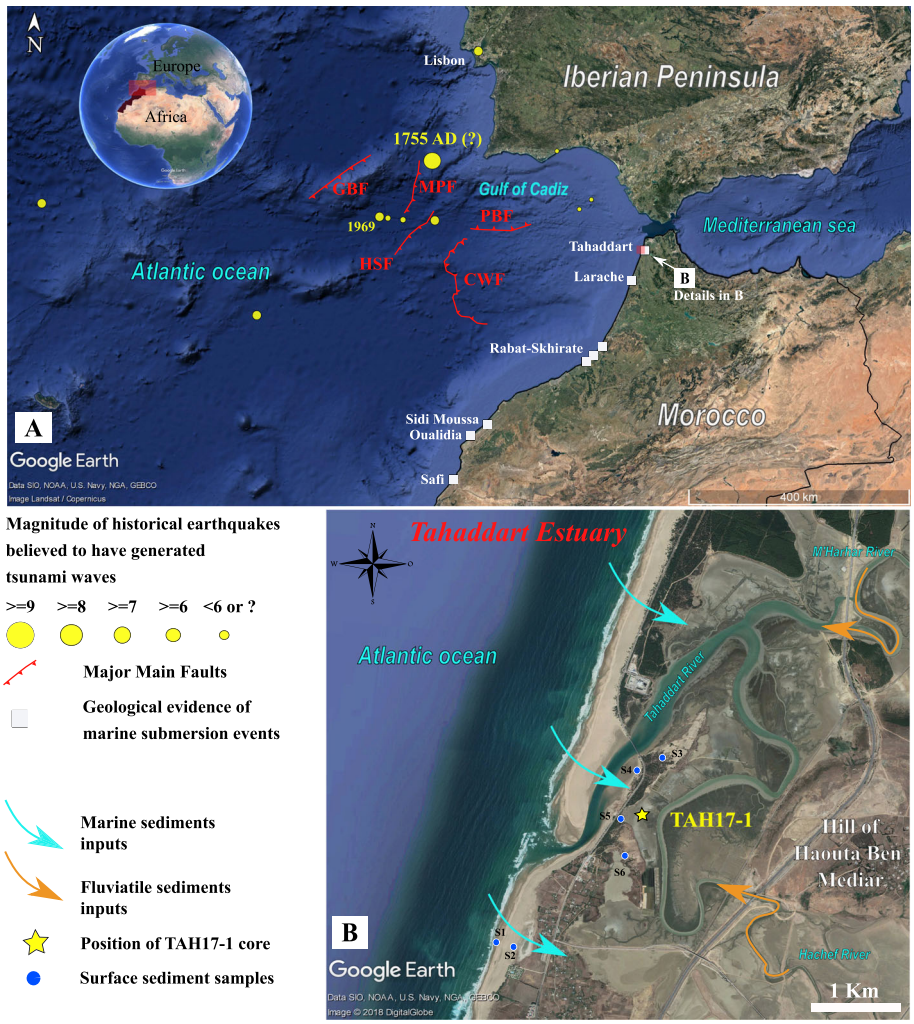


Fig. 1 a Google Earth image showing the Gulf of Cadiz. Historical data of seismic events generating (or believed to have generated) tsunami waves are from NOAA's National Centers for Environmental Information (NCEI 2020). They are presented as yellow dots with magnitude ranging between 6 and 9. Potential tsunamigenic faults (red traces) in the Gulf of Cadiz are simplified from Omira et al. (2009). White squares illustrate onshore geological evidences of marine submersion events along the Atlantic coast of Morocco

Tahaddart estuary in September 2017 with the following geographical coordinates: 35°34′30.94″N, 5°59′7.79″W (Fig. 1). The distance between the coring site and the shoreline is approximately 1 km. The coring operation was conducted using a "Cobra" portable percussion corer and a hydraulic puller (Géosciences Montpellier Laboratory, France). Once in the laboratory, the core was split lengthwise, photographed, logged and then subsampled for further analysis.

In order to study all sources of sediment that contribute to the filling of the Tahaddart estuary, thirty-nine surface sediment samples were collected during another field mission from the high Tahaddart River watershed to the coastal area (beaches and dunes) (Fig. 2).

Grain size

Laser grain-size analyses were carried out in each centimeter along the TAH17–1 core using a Beckman-Coulter LS13320 (Géosciences Montpellier Laboratory, France). Prior to analysis, in order to prevent flocculation, samples were suspended in deionized water and exposed to ultrasound during the measurement for 90 s. Each sample was measured twice to ensure accurate and consistent results. According to Friedman and Sanders (1978), the particle sizes obtained are classified into three categories (clay, silt and sand). Grain-size parameters (D50 and sorting) were calculated according to the geometric method of moments using GRADISTAT software (Blott and Pye 2001). Additional grain-size measurements were performed on

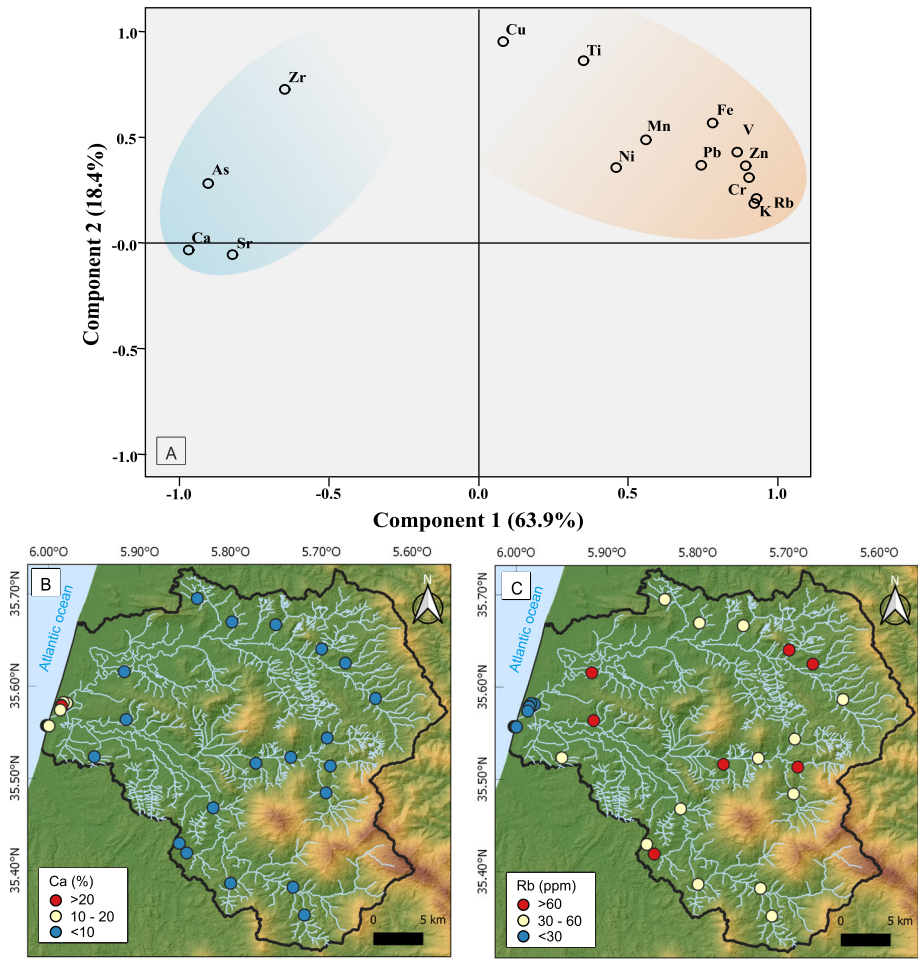


Fig. 2 a Principal Component Analysis of geochemical data from coastal and watershed surface samples. **b**,**c** Maps of Calcium and Rubidium contents around the Tahaddart estuary

coastal surface samples using the same procedure mentioned above.

Geochemistry

Geochemical analysis was carried out using a hand-held Niton XL3t spectrometer (pXRF; Geoscience Montpellier Laboratory, France). The device was calibrated first through powdered standards and measurements were performed directly in each centimeter of the half-core. To avoid contamination when changing the measuring point, the core was covered with a thin layer of ultralene film (Richter et al. 2006). Each measurement was taken for 150 s with the soil mode, which is the most suitable mode for unconsolidated sediments.

Additionally, geochemical analysis using the same device in a fixed position was conducted also on surface samples to geochemically distinguish all sources of sediments arriving to the Tahaddart estuary. Before measurements were taken, all samples were dried and grounde to < 63 μm using a mechanical agate mortar, and then prepared in classic XRF sample cups covered with a thin ultralene film. We maintained 150 s for each measurement with soil mode.

Geochronology ($^{210}Pb_{ex}$, ^{137}Cs and ^{14}C)

Radiochronological data for the last century was obtained using ^{137}Cs and $^{210}Pb_{ex}$ measurements with a CANBERRA BEGe 3825 gamma spectrometer (Géoscience Montpellier Laboratory, France). Samples were collected in the first 30 cm. The ^{137}Cs activity vs. depth distributions was done according to Robbins and Edgington (1975), while CFCS ("Constant Flux, Constant Sedimentation rate") model was used for the $^{210}Pb_{ex}$ (Golberg 1963; Krishnaswamy et al. 1971). In order to complete the chronology over longer periods of time, ^{14}C dates were performed on 5 marine shells in the LMC14 laboratory (the ARTEMIS accelerator mass spectrometry at the CEA Institute in Saclay (Atomic Energy Commission)) according to the procedure described

by Tisnérat-Laborde et al. (2001). We calibrated the ^{14}C dates using the CALIB 7.1 program (Stuiver et al. 2017).

Results

Sediment sources

The XRF spectrometer is designed to detect the concentration of about 30 chemical elements. From the surface sample results, we only retained those with interpretable concentrations, which were Potassium (K), Chromium (Cr), Vanadium (V), Zinc (Zn), Lead (Pb), Iron (Fe), Manganese (Mn), Nickel (Ni), Zirconium (Zr), Calcium (Ca), Strontium (Sr), Titanium (Ti), Copper (Cu) and Arsenic (As). A Principal Component Analysis (PCA) was performed on this set of data, made of 15 variables (selected chemical elements) and 39 samples in order to geochemically characterize all sources of sediment arriving at the Tahaddart estuary. As a result, the first and second PCA factors explain respectively 63.9% and 18.4% of the total variance. We noticed the presence of two chemical poles: (1) a first one gathering Rb, K, Cr, V, Zn, Pb, Fe, Mn, Ni, Ti and Cu, and (2) a second one regrouping Ca, Sr, As and Zr (Fig. 2).

Mapping the concentration of Rb (pole 1) and Ca (pole 2) allowed us to spatially locate these two sources of sediment (Fig. 2). On the one hand, samples situated on the watershed are rich in Rb (> 30 ppm) and poor in Ca (< 10 ppm), which pinpoints that elements from the first pole can be used to trace fluvial sediment inputs into the Tahaddart estuary. The richness of watershed samples with terrigenous elements like Rb, Fe and Ti can be explained by the silico-clastic nature of the rocks forming the watershed (Durand-Delga and Kornprobst 1985). On the other hand, coastal samples collected from the beach and dune system exhibit high Ca (> 10 ppm) and low Rb (< 30 ppm) concentrations, suggesting that elements from the second pole can be used to detect marine sediments arriving to the coring site through high-energy events (storm surges or tsunamis). This confirms the mineralogical observations conducted by El Talibi (2016) on a set of coastal surface samples from the Tahaddart estuary (dune and beach). The author reports the presence of gastropod shells, foraminifera and other shell debris, which explains the high Ca concentrations in our coastal samples. The same study highlighted the presence of heavy minerals such as pyroxene, andalusite, staurolite and kyanite. Zircon was also present, but with a small percentage (El Talibi 2016). The latter would be the source of Zr in our samples.

Core description

The visual description of the core TAH17–1 with both the grain-size and pXRF measurements allowed the identification of four sedimentary units (Fig. 3).

Unit a (270–193 cm depth)

Overall, unit A is dominated by shelly, silty brown sands. From 270 to 210 cm, we have a fining upward sequence, ranging from poorly sorted medium sand (D50: 200–400 μm; sorting: 2–4 μm) to very poorly sorted sandy silt (D50: 7–30 μm; sorting 4–9 μm). After that, between 210 and 193 cm, it evolves into very poorly sorted fine sand (D50: 100-200 μm; sorting 4–9 μm). Note that the high values of mud content observed at 247 cm are due to rounded mud rip-up clasts (3 × 4 cm in size). On the one hand, the Ca content follows perfectly the D50 profile by decreasing upward from 130,000 to 55,000 ppm. The Zr, on the other hand, shows high values at 270–248 cm and 227–195 cm depth, with a maximum concentration around 1800 ppm at 253 and 214 cm depth. The low content of fine sediments is reflected through a low concentration of Rb, with values between 5 and 30 ppm.

Unit B (193–140 cm depth)

Unit B presents a relatively sharp contact with the underlying unit (A). It is dominated by a dark grey silty clay deposit with several intercalations of poorly to very poorly sorted muddy sand layers (D50: 100–200 μm; sorting: 3–7 μm). These allochthonous sandy levels are very thin (< 4 cm) and have no particular sedimentary structure. However, a minor deformation of these layers can be reported due to the friction of the sediment with the inner walls of the PVC pipe during the coring operation. Compared to the prevailing muddy sedimentation, these sandy layers are rich in Ca and Zr with maximum values around 45,000 and 500 ppm, respectively.

Unit C (140–125 and 92–87 cm depth)

As a result of a shortening process affecting segments 1 and 2 of the core (0–100 cm and 100–200 cm), unit C was separated into two parts: 140–125 cm and 92–87 cm. It is marked by chaotic and structureless brown sediments, ranging from silt to pebbles, especially the first 15 cm (140–125 cm). The contact with the underlying unit (B) is sharp and erosional, marked by the presence of grey mud clast (2.5 × 3.5 cm in size). No sedimentary structures are obvious through grain size statistics for unit C. The Ca and Rb show the same pattern, decreasing upward from 45,000 to 4000 ppm and from 55 to 30 ppm, respectively. The Zr remains low between 140 and 125 cm, with values around 200 ppm, then increasing significantly at the end of the unit with a maximum value of 1080 ppm.

Unit D (87–0 cm depth)

Unit D represents the topmost unit. It is completely dominated by brown mud fraction up to 100% with traces of oxidized plant roots between 30 and 87 cm

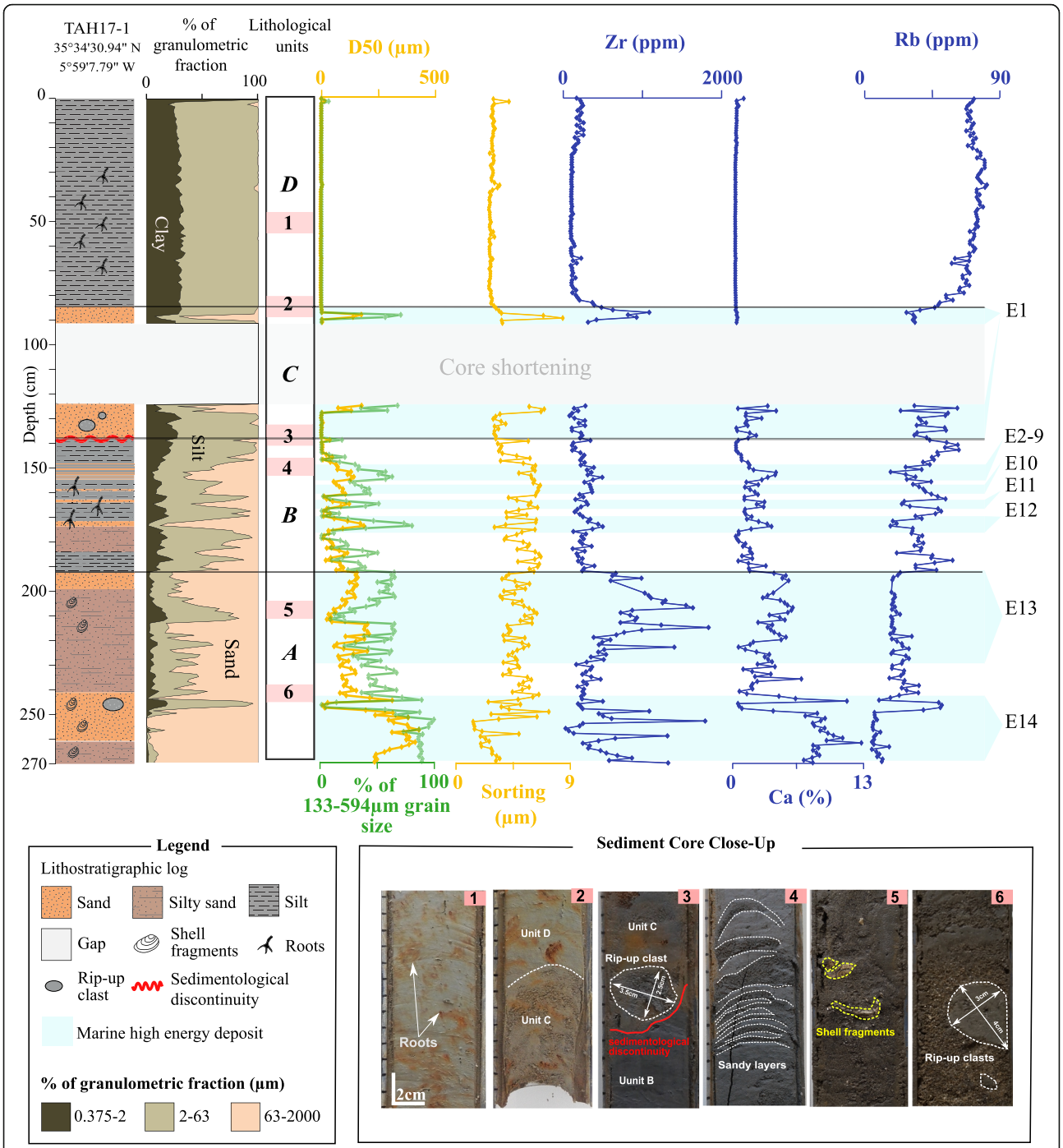


Fig. 3 Schematic log of the TAH17–1 core with grain size parameters (Cumulative grain size %, 133-594 µm fraction, D50 and sorting) and geochemical profiles of Ca, Zr and Rb

depth. This abundance of fine sediment translates into high values of Rb around 80 ppm (the highest in the core). The concentrations of Ca and Zr are low with values around 2000 and 100 ppm, respectively. This reflects the predominance of river sedimentation over the marine one.

Geochronology

The chronological results for our record were obtained using radiometric dating techniques. On a centennial time scale, we used a combination of two short-lived radionuclides: $^{210}Pb_{ex}$ and ^{137}Cs. In the case of undisturbed sediments, an increasing amount

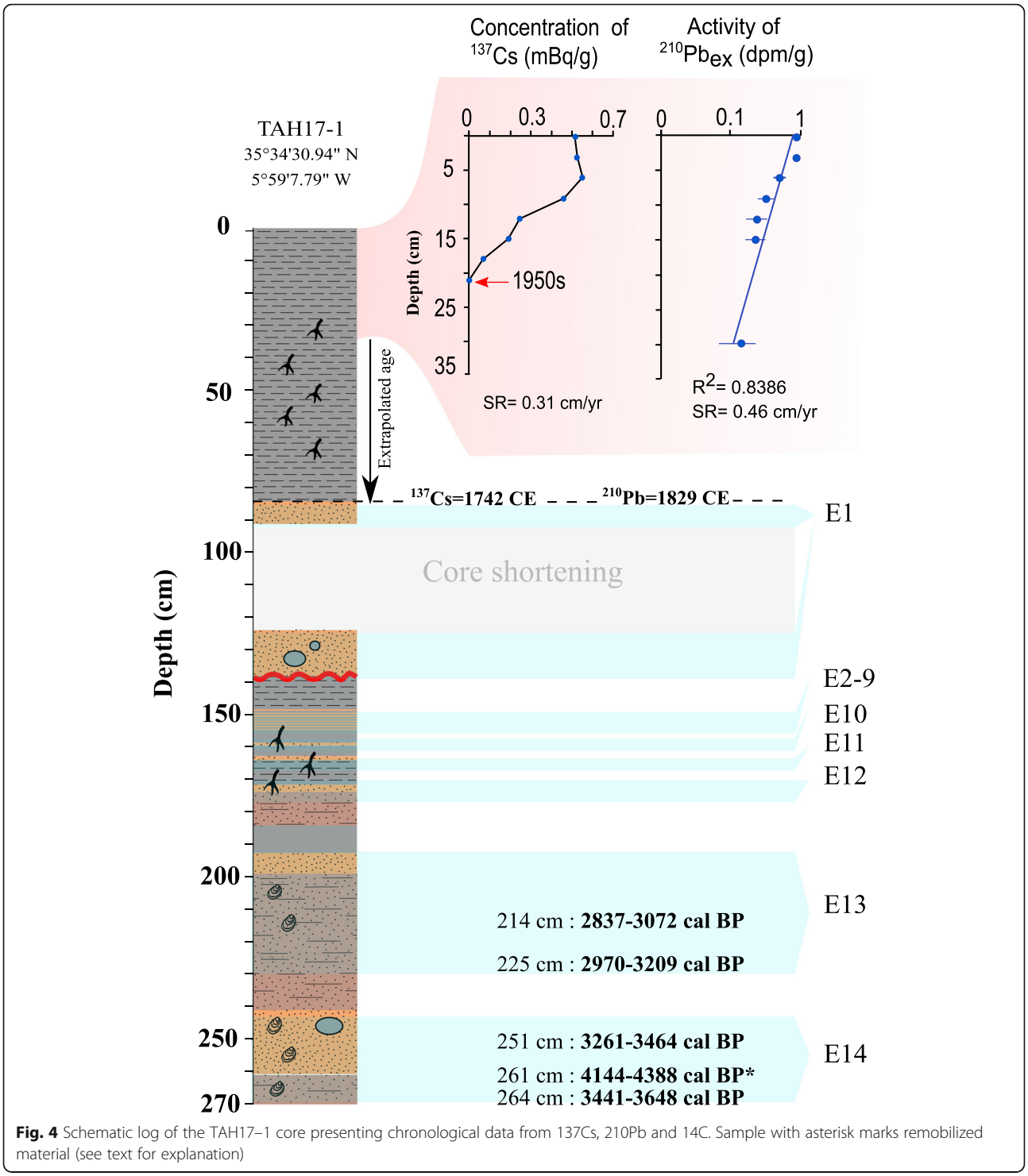


Fig. 4 Schematic log of the TAH17–1 core presenting chronological data from 137Cs, 210Pb and 14C. Sample with asterisk marks remobilized material (see text for explanation)

of ^{137}Cs coincides with the beginning of nuclear testing in the 1950s, and the highest values in the sediment sequence correspond to the maximum atmospheric intensity reached in 1963 CE, as a result, the sedimentation rate can be calculated using these two temporal markers (Fig. 4). On the other hand, the concentration of ^{210}Pb$_{ex}$ decreases exponentially with depth and the sedimentation rate is calculated by dividing 0.03108 (the ^{210}Pb decay constant) by the slope of exponential best fits (Golberg 1963; Krishnaswamy et al. 1971). In the TAH17–1 core, the main factors that can impact sedimentation rates such as

bioturbation (Cochran 1985), grain size effects (Chanton et al. 1983) or instantaneous events (Smith and Walton 1980; Arnaud et al. 2002) were unobserved in the first 40 cm (sampling interval). The sedimentation rate for the ^{137}Cs was calculated based only on the 1950s marker located at a depth of 21 cm, resulting in a rate of 0.31 cm/year. The sedimentation rate obtained through $^{210}Pb_{ex}$ is equal to 0.46 cm/year, which gives an average value of 0.38 cm/year between the two methods. This slight difference between the two sedimentation rates is likely a result of the limited number of samples analyzed or potentially the impact of artificial external actions such as sea salt production units (located in the area), which can induce reworking and mixing of superficial sediments.

On a millennial time scale, five marine shells sampled from the TAH17–1 core were dated using conventional Accelerator Mass Spectrometry (AMS) ^{14}C measurements. To calibrate these samples, the first step is to evaluate the modern reservoir age R(t) and its regional deviation ΔR. For this purpose, two additional samples composed with a marine shell and a piece of wood were added to the analyzed samples (referenced as SacA 54, 447 and SacA 54,446, respectively). These additional samples were taken from another core collected for dating purposes near our coring site. In order to limit the probability of ending up with old remobilized materials, they are from the same clayey silty level. Despite the fact that both samples have the same age of deposition, the ^{14}C value of the marine shell (i.e. 1105 ± 30 BP) is older than the piece of wood (i.e. 810 ± 30 BP); this difference is due to the effect of the marine reservoir age R(t), which corresponds to 295 years in our case. Based on the Intcal13 curve (Reimer et al. 2013), we can estimate a historical age for the marine shell using the atmospheric ^{14}C value of the wood (1240 CE; Reimer et al. 2013). The ΔR value is then calculated by subtracting the marine model age value, estimated at 1240 CE (1180 ± 24 ^{14}C years; Reimer et al. 2013), from the measured apparent ^{14}C age of the marine shell (1105 ± 30 BP years; Table 1), which corresponds to − 75 ± 20 years (Table 1). This value is close to the one proposed by Monge Soares and Matos Martins (2010) from the Andalusian coast (Spain), which is equivalent to − 135 ± 20 years. Nevertheless, our calculated ΔR must be taken with caution and more studies are needed to determine a mean value to be used with marine calibration curves. Thus, the five marine shells collected from the TAH17–1 core were calibrated using the CALIB 7.1 program (Stuiver et al. 2017) with a ΔR value of − 75 ± 20 years. The results are reported in Table 2 with an error range of 2σ. Note that sample n°4 must be a remobilized material from older sediments since sample n°5 taken from lower sedimentary level has a younger age. The TAH17–1 covers approximately the last 3600 years.

Discussion

Identification of marine submersion deposits

Geochemical and grain-size observations on the TAH17–1 core show a sedimentary sequence dominated by silty-clayey deposits and interrupted over time by injections of multiple allochthonous coarse materials. To pinpoint the source of these sandy layers, we first compared their geochemical attributes with those from surface samples. This allowed us to determine whether these deposits are coming from the watershed through river floods or from the coast during storm surges and tsunamis. As expected, all sandy levels existing in the TAH17–1 core have a good geochemical correlation with coastal surface samples; both show enrichment with Ca and Zr and a depletion with Rb, which reveals a marine source for these high-energy deposits (Figs.2 and 3).

The "grain-size vs. standard deviation" diagram developed by Boulay et al. (2003) was used to recognize the grain size population of these sandy levels. The method allows the identification of the grain size ranges with the highest variability along a sedimentary sequence. For each of the 92 grain-size intervals given by the Beckman-Coulter LS13 320, standard deviations (SD) were calculated for our 238 samples. As a result, the grain-size versus standard deviation displayed in Fig. 5 shows two main populations with high variability (SD > 1) in the TAH17–1 core. The first is between 1 and 9 μm (clay to fine silt) and the second between 133 and 594 μm (fine to coarse sand). By comparing the "grain-size vs standard deviation" diagram with the grain-size distributions of coastal surface samples, we have observed a positive correlation between the two diagrams (Fig. 5). This demonstrates that the 133–594 μm class can be used as a proxy to trace coarse sediments arriving at the estuary during marine submersion episodes.

Table 1 Estimation of marine reservoir age R(t) and its regional deviation ΔR using 14C ages on wood and marine shell

Lab code	Material dated	^{14}C age (BP)	Historical age using Intcal13 curve	Marine reservoir age R(t) (years)	Model age (Marine13 curve)	ΔR (Years)
SacA 54, 447	Marine shell	1105 ± 30	1240 CE	295	1180 ± 24	−75 ± 20
SacA 54, 446	wood	810 ± 30				

Table 2 Calibrated ^{14}C ages of samples taken from the TAH17–1 core. Sample with asterisk marks remobilized material (see text for explanation)

N°	Lab code	Depths (cm)	Dated material	δ13C (‰)	^{14}C age (BP)	^{14}C age (cal BP) (two sigma ranges) [start:end]
1	SacA 54,435	214	Marine shell	−1,90	3090 ± 30	[cal BP 2837: cal BP 3072]
2	SacA 54,436	225	Marine shell	−2,30	3195 ± 30	[cal BP 2970: cal BP 3209]
3	SacA 54,433	251	Marine shell	4,10	3415 ± 30	[cal BP 3261: cal BP 3464]
4	SacA 54,437	261	Marine shell	−2,40	4105 ± 30	[cal BP 4144: cal BP 4388][a]
5	SacA 54,434	264	Marine shell	3,50	3570 ± 30	[cal BP 3441: cal BP 3648]

[a]Age inversion

By connecting the geochemical profiles of Ca, Zr and Rb with the 133-594 μm grain-size curve, we have uncovered 14 high-energy marine levels from the TAH17–1 core, termed from the top to the base as E1-E14 (Fig. 3). These deposits are all distinguished by a high percentage of the 133–594 μm fraction, as well as a high concentration of marine geochemical tracers (Ca and Zr). From 0 to 190 cm, it was easy to distinguish the E1-E12 levels due to the strong contrast between these coarse sandy deposits and the fine background

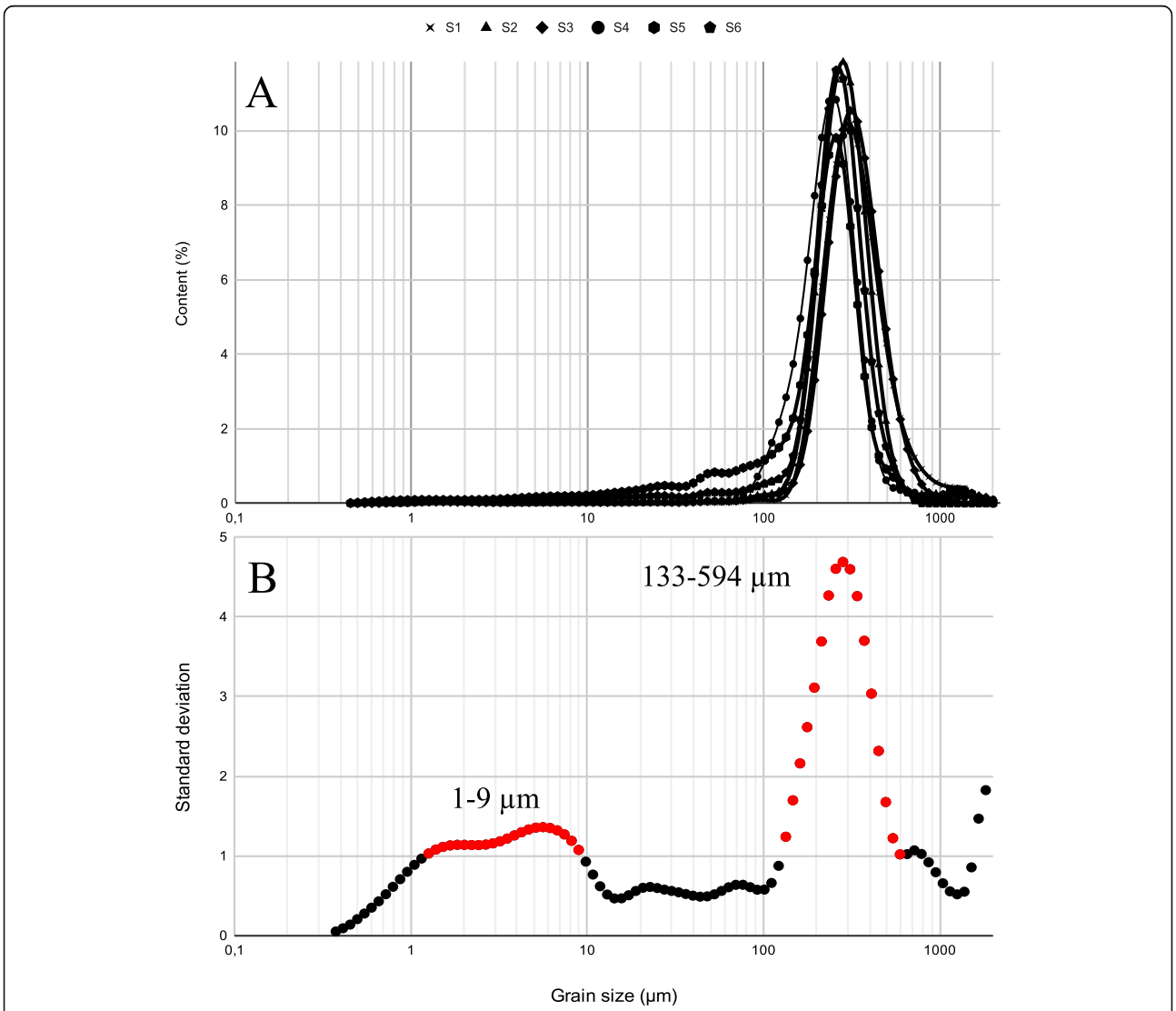


Fig. 5 a Grain size measurements of costal surface samples. **b** Standard deviation values vs. grain size classes of core TAH17–1 with red dots representing populations with the highest variability between 1 and 9 μm and between 133 and 594 μm

sedimentation. From 190 to 270 cm, it was difficult to place the boundaries for E13 and E14. Indeed, the grading curve does not show a clear limit between these two layers. Consequently, we used as reference, the two Zr peaks between 270 and 248 cm and 230–190 cm to determine the boundary of these two deposits (Fig. 3).

In addition to the two selection criteria mentioned above (grain-size and geochemistry), the E1 and E14 levels show other familiar macroscopic sedimentary structures of marine submersion deposits (Fig. 2; Table 3). The E1 level displays a chaotic structure with the presence of rock fragments and muddy rip-up clasts. It is also separated from the underlying sediments by a net erosion surface, marked by an abrupt change in sediment color from dark grey to dark brown. The E14 level also has additional indicators in the form of muddy rip-clasts and a slight normal grading. The establishment of these macroscopic sedimentary structures requires strong hydrodynamic conditions, like the one provided by storm surges and tsunamis (Morton et al. 2007).

Site sensitivity across time

On a millennial time scale, the paleoenvironmental evolution of a coastal zone can change its sensitivity to overwash deposition. Variation in relative sea level, inlets position and sediment supply can alter the frequency and intensity of events recorded in a sediment archive (Scileppi and Donnelly 2007; Dezileau et al. 2011; Woodruff et al. 2013).

Evolution of relative sea level controls the advance or retreat of coastlines. Thus, an increased number of sand layers in a sediment core can be the result of a relative sea level change. Studies concerning Holocene sea level fluctuations along the Moroccan Atlantic coast remain very limited. Early works conducted by Gigout (1959) and Delibrias (1973) have suggested a 2 m drop in relative sea level during the last 6000 years, which is small and probably not enough to completely change the deposition environment of the Tahaddart estuary. On top of that, Sedimentation in the TAH17–1 core started 3600 years ago, so the relative sea level was definitely lower at that moment, and its influence on the sediment record was probably even weaker. However, the core presents a sedimentary sequence dominated by fine-grained sediments (clay and silt), suggesting that the Tahaddart estuary has succeeded in maintaining a low-energy environment during this period of time (Fig. 3). The proxies used in this study (grain-size and

Table 3 Sedimentological characteristics of marine submersions deposits along the TAH17–1 core

Events	Position in the core (cm)	Thickness (cm)	Grading	Sorting	Upper Contact	Basal contact	Other sedimentological characteristics
E1	87–92 125–140	20	No (chaotic structure)	Very poorly sorted	Relatively sharp	Sharp (erosional)	Angular gravels and Mud-clasts
E2	148–149	1	No	Very poorly sorted	Sharp	Sharp	No
E3	150–151	1	No	Very poorly sorted	Sharp	Sharp	No
E4	152–153	1	No	Very poorly sorted	Sharp	Sharp	No
E5	154–155	< 1	No	Very poorly sorted	Sharp	Sharp	No
E6	154–155	< 1	No	Very poorly sorted	Sharp	Sharp	No
E7	155–156	< 1	No	Very poorly sorted	Sharp	Sharp	No
E8	155–156	< 1	No	Very poorly sorted	Sharp	Sharp	No
E9	156–157	1	No	Very poorly sorted	Sharp	Sharp	No
E10	159–160	1	No	Very poorly sorted	Slightly Sharp	Slightly Sharp	No
E11	163.5–165	1,5	No	Very poorly sorted	Slightly Sharp	Slightly Sharp	No
E12	172–175	3	No	Very poorly sorted	Slightly Sharp	Slightly Sharp	No
E13	190–230	40	Unclear	Very poorly sorted	Sharp	Gradational	No
E14	248–270	22	Normal grading	Poorly sorted	Gradational	Not found	Mud-clasts

geochemistry), as well as the sedimentary indicators (rip-up clasts, grading), showed that all sandy coarse peaks present within the TAH17–1 core were deposited through marine high-energy events rather than changes in relative sea level.

The presence of inlets near a coring site can facilitate the arrival of marine waters to the latter during high-energy events, thus increasing its sensitivity to overwash deposition. Currently, the mouth of the Tahaddart River, which is in close proximity to our coring site, is the only way for marine waters to enter the estuary during tidal movements. The available cartographic and satellite data on the Tahaddart estuary cover only the last 100 years. They show a stable position of the river's mouth during this period. However, on a larger time scale (last 3600 years), its position has certainly changed. Information can be inferred through the evolution of the sandy spit present at the mouth of the Tahaddart River. In response to the coastal drift, this sandy spit evolves from North to South, causing the river's mouth to deviate progressively in its direction. As a result, we can deduce the river's entrance was previously further north, and couldn't influence the geological record of our high-energy deposits.

A decrease in sediment inputs from the watershed may lead to a degradation of the barrier beaches at the study site, making it easily submersible during marine high-energy events. The construction of the Ibn Batouta dam in 1977 was the beginning of a progressive decrease in sedimentary inputs from the Tahaddart watershed (Achab 2011). However, the sensitivity of the coring site has remained unchanged over the last 40 years. Indeed, the first 30-40 cm of the core, covered with the ^{137}Cs activity, show no sign of high-energy deposits. Consequently, the factor of sedimentary inputs has no impact on our results.

Comparison with historical archives

The results obtained so far confirm that the Tahaddart estuary has been confronted with episodes of marine submersion during the last 3600 years. Differentiating now between storm and tsunami deposits is a delicate question, especially when you rely on a single core. Chronological correlation of our sedimentary deposits with available historical archives can give more information about events responsible for these deposits such as magnitude, wave run-up, source, causal damages, but most important, it helps with the precise dating of these deposits. However, if we take into consideration the distance between the coring site and the coastline (about 1 km), we believe that only tsunamis are strong enough to transport sediment as far. Satellite images from Google Earth have shown that the last storm of 2014 (considered a major event) did not overwash sediments to the TAH17–1 core. This may also have been the case for previous storms. Based on that, as a first step, we have chosen to correlate our dated deposits only with tsunami records from the Moroccan and Iberian Atlantic coasts (Fig. 6).

Deposits E13 and E14 were dated based on the results of ^{14}C. The former was established between 2837 and 3209 cal BP, whereas the latter was placed between 3261 and 3648 cal BP. The correlation of these two deposits with the Moroccan geological archives remains inconclusive, as the available studies lack chronological precision (Fig. 6). On the Iberian Atlantic coast (Spain and Portugal), marine submersion deposits with the same age as E13 and E14 have been reported in Spain's Tinto-Odeil and Guadalquivir estuaries, as well as the Bay of Cadiz (Lario et al. 2011, and references therein; Ruiz et al. 2013, and references therein). The presence of these contemporary deposits in two different countries allows us to hypothesize the existence of a regional event around 3200 cal BP, probably a tsunami type. In this case, E13 and E14 deposits evince either a tsunami event with one flood wave and two flow stages (inflow and backflow), similar to the one described by Higman and Bourgeois (2008) along the Nicaraguan Coast, or a tsunami event with two flood waves (two inflows) like the tsunami deposits reported by Nanayama (2008) within the alluvial plain of Taisei, Japan. Accordingly, the muddy sand layer separating E13 and E14 (205-215 cm) is considered as mud drape (Fig. 3), and probably implemented as a result of low energy conditions between the inflow and backflow, or between the two inflows (Fujiwara and Kamataki 2007). However, there is still room for verification to confirm or refute our interpretation. We prefer to maintain E13 and E14 as separate events until further studies are conducted.

We were unable to give an age for E2-E12 events due to the lack of ^{14}C datable material in the TAH17–1 core. A combination of radiocarbon and luminescence dating techniques can be more efficient, since the latter has been applied successfully to date tsunami deposits on the Spanish and Portuguese coasts (Dawson et al. 1995; Koster and Reicherter 2014).

The uppermost layer (E1) was dated using extrapolated ages from ^{137}Cs and $^{210}Pb_{ex}$ concentration profiles. Indeed, since we have a homogeneous deposit between the top of the core and the top of the E1 layer (0–85 cm depth), we can assume that we have a constant sedimentation rate for this horizon. The linear extrapolation of sedimentation rates from ^{137}Cs

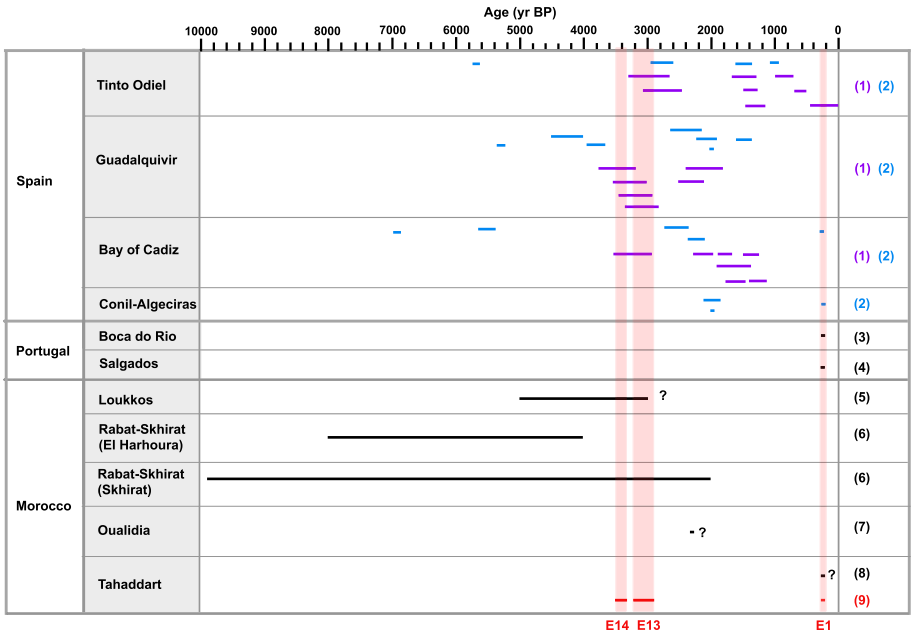


Fig. 6 Chronological correlation of dated events in TAH17–1 core with other on-shore deposits along the Atlantic coast of Spain, Portugal and Morocco. (1) Tsunamigenic deposits summarised by Ruiz et al. (2013). (2) Tsunamigenic deposits summarised by Lario et al. (2011). (3) (Dawson et al. 1995) (4) (Costa et al. 2012). (5) (Mhammdi et al. 2015). (6) (Chahid et al. 2016). (7) (Mellas 2012). (8) (El Talibi et al. 2016). (9) This study (Khalfaoui et al.,). The question marks indicate an estimated age

and $^{210}Pb_{ex}$ gives an age of 1742 +/− 30 CE and 1829 +/− 30 CE respectively, with an average of 1785 CE. According to historical records, the best candidate for this deposit would be the 1755 CE tsunami, known as the Lisbon tsunami, wish is a well-documented regional event that devastated the Moroccan and Iberian Atlantic coasts (Kaabouben et al. 2009; Blanc 2011). This tsunami was generated by an earthquake of magnitude 8.3 with wave heights between 3 and 15 m on the Moroccan Atlantic coast (Martínez Solares and López Arroyo 2004; Blanc 2009). Sedimentary deposits from this event have already been identified and dated on the Iberian Atlantic coast (Dabrio et al. 1998; Vigliotti et al. 2019). For the Moroccan side, to our knowledge, no sedimentary deposit has been ascribed to this event through chronological data, which allows us to consider E1 as the first dated sedimentary trace of the Lisbon tsunami on the Moroccan coasts.

Between E1 and the present day, no high-energy deposits were recorded in the TAH17–1 core. The Lisbon tsunami has probably led to major morphological changes in the coastal dunes protecting the study site. The latter is becoming more insulated from marine high-energy events as a result of this tsunami. Small marine submersion episodes similar to the tsunami of 1969 CE and the storm of 2014 CE are no longer able to overcome this natural obstacle.

Conclusion

Our study presents a 3600 year record of past marine submersion events using a high-resolution multi-proxy analysis on a sediment core retrieved from the Tahaddart estuary (NW of Morocco). The sedimentary sequence has revealed the presence of 14 sandy layers trapped in fine estuarine sediments (E1-E14). These allochthonous levels share the same geochemical and granulometric features as surface samples collected from the Tahaddart coast. Indeed, both show enrichment with marine geochemical tracers (Ca and Zr) and have the same grain-size fraction (133-549 μm), which illustrates a marine source for these sandy layers.

Among these marine submersion deposits, three have been dated using conventional dating methods (^{210}Pb, ^{137}Cs and ^{14}C), which are E1, E13 and E14. The most recent deposit (E1) has been dated around 1785 CE and was related to the great tsunami of Lisbon in 1755. The E1 layer represents the first dated deposit of this event along the Atlantic coast of Morocco. The E13 and E14 (oldest deposits) were established by an event dated around 3200 BP, whose sedimentary traces have also been reported in several locations along the Spanish Atlantic coast.

These initial results aim to set the context for more detailed future studies along the Tahaddart estuary, in order to demonstrate its potential to record marine

submersion events. The combination between cross-shore and long-shore cores, coupled with more proxies, like Anisotropy of Magnetic Susceptibility (AMS) and microfaunal analysis, can provide more information about these deposits identified with the TAH17–1 core. The two dated events in this paper will feed the regional database on past extreme sea events, especially along the Moroccan Atlantic coasts, where there is a lack of studies on this topic. The objective is to assist coastal managers to develop proactive adaptation strategies to protect the coastal population from future damages that can be caused by these events.

Acknowledgements
The authors would like to thank Professor Raphaël Paris for his valuable comments which helped to improve the quality of the manuscript. All thanks to the Laboratoire de Mesure ^{14}C (LMC14) ARTEMIS at the CEA Institute at Saclay (French Atomic Energy Commission) for the ^{14}C analyses.

Authors' contributions
All authors performed the fieldwork. OK conducted the experiments, analyzed the data and wrote the first draft of the manuscript. LD conceived the study and revised the manuscript and data analysis. JPD helped with the grain-size experiments and contributed to the manuscript revision and analysis. MS participated in the design and coordination of the study and helped to interpret the results. All of the authors drafted, read and approved the final manuscript.

Funding
This study was funded by MISTRALS/PALEOMEX project and the Partenariat Hubert Curien (PHC) Toubkal (No. TBK/17/40 - Campus No. 36864YB; coordinated by Laurent Dezileau and Maria Snoussi).

Availability of data and materials
The datasets used and/or analyzed during the current study are available from the corresponding author on reasonable request.

Competing interests
The authors declare that they have no conflict of interest.

Author details
[1]Normandie Univ, UNICAEN, UNIROUEN, CNRS, M2C, 14000 Caen, France. [2]University Mohammed V in Rabat, Institut Scientifique, Laboratory LGRN and GEOPAC Research Centre, Av. Ibn Batouta, B.P. 703 Agdal, Rabat, Morocco. [3]ASM UMR5140, Université Montpellier 3, CNRS, MCC, 34199 Montpellier, France.

Received: 27 February 2020 Accepted: 4 November 2020
Published online: 12 November 2020

References

Abadie SM, Harris JC, Grilli ST, Fabre R (2012) Numerical modeling of tsunami waves generated by the flank collapse of the Cumbre Vieja Volcano (La Palma, Canary Islands): Tsunami source and near field effects. J Geophysical Res Oceans 117:n/a–n/a https://doi.org/10.1029/2011JC007646

Achab M (2011) Les plages et les vasières des environs des embouchures des oueds Tahaddart et Gharifa (NW du Maroc): dynamique morphosédimentaire et impact des aménagements sur leur évolution récente. In: Sandy beaches and coastal zone management. Proceedings of the Fifth International Symposium on Sandy Beaches, vol 6. Travaux de l'Institut Scientifique, Rabat, pp 1–12

Aitali R, Snoussi M, Kasmi S (2020) Coastal development and risks of flooding in Morocco: the cases of Tahaddart and Saidia coasts. J Afr Earth Sci 164:103771 https://doi.org/10.1016/j.jafrearsci.2020.103771

Arnaud F, Lignier V, Revel M, Desmet M, Beck C, Pourchet M, Charlet F, Trentesaux A, Tribovillard N (2002) Flood and earthquake disturbance of 210Pb geochronology (Lake Anterne, NW Alps). Terra Nova 14:225–232 Wiley Online Library. https://doi.org/10.1046/j.1365-3121.2002.00413.x

Blanc PL (2009) Earthquakes and tsunami in November 1755 in Morocco: a different reading of contemporaneous documentary sources. Nat Hazards Earth Syst Sci 9:725–738 https://doi.org/10.5194/nhess-9-725-2009

Blanc PL (2011) The Atlantic tsunami on November 1st, 1755: world range and amplitude according to primary documentary sources. In: The Tsunami Threat - Research and Technology InTech https://doi.org/10.5772/14605

Blott SJ, Pye K (2001) GRADISTAT: a grain size distribution and statistics package for the analysis of unconsolidated sediments. Earth Surf Processes Landforms 26:1237–1248 Wiley Online Library. https://doi.org/10.1002/esp.261

Boughaba A (1992) Les littoraux meubles septentrionaux de la peninsule de Tanger (Maroc): Geomorphologie et effet de l'intervention anthropique sur leur environnement. Universite de Nantes

Boulay S, Colin C, Trentesaux A, Pluquet F, Bertaux J, Blamart D, Buehring C, Wang P (2003) Mineralogy and sedimentology of pleistocene sediment in the South China Sea (ODP site 1144), vol 184, pp 1–21

Chahid D, Lenoble A, Boudad L, Vliet-Lanoë BV (2016) Enregistrements sédimentaires d'événements de haute énergie, exemples de la côte atlantique de Rabat-Skhirat (Maroc). Quaternaire:155–169 https://doi.org/10.4000/quaternaire.7543

Chanton JP, Martens CS, Kipphut GW (1983) Lead-210 sediment geochronology in a changing coastal environment. Geochimica Cosmochimica Acta 47:1791–1804 Elsevier. https://doi.org/10.1016/0016-7037(83)90027-3

Cochran JK (1985) Particle mixing rates in sediments of the eastern equatorial Pacific: Evidence from 210Pb, 239,240Pu and 137Cs distributions at MANOP sites. Geochimica Cosmochimica Acta 49. Elsevier:1195–1210 https://doi.org/10.1016/0016-7037(85)90010-9

Costa PJM, Andrade C, Freitas MC, Oliveira MA, Lopes V, Dawson AG, Moreno J, Fatela F, Jouanneau JM (2012) A tsunami record in the sedimentary archive of the Central Algarve coast, Portugal: characterizing sediment, reconstructing sources and inundation paths. The Holocene 22:899–914 https://doi.org/10.1177/0959683611434227

Dabrio CJ, Goy JL, Zazo C (1998) The record of the tsunami produced by the 1755 Lisbon earthquake in Valdelagrana spit (Gulf of Cádiz , southern Spain). Geogaceta 23:31–34

Dawson AG, Hindson R, Andrade C, Freitas C, Parish R, Bateman M (1995) Tsunami sedimentation associated with the Lisbon earthquake of 1 November AD 1755: Boca do Rio, Algarve, Portugal. The Holocene 5:209–215 https://doi.org/10.1177/095968369500500208

Degeai JP, Devillers B, Dezileau L, Oueslati H, Bony G (2015) Major storm periods and climate forcing in the Western Mediterranean during the Late Holocene. Quat Sci Rev 129:37–56 https://doi.org/10.1016/j.quascirev.2015.10.009

Delibrias, G. 1973. Variation du niveau de la mer sur la cote ouest africaine, depuis 26.000 ans. Paris, CNRS, coll. Inter., Variat. Clim. Pleist 219: 127–134

Dezileau L, Sabatier P, Blanchemanche P, Joly B, Swingedouw D, Cassou C, Castaings J, Martinez P, Von Grafenstein U (2011) Intense storm activity during the little ice age on the French Mediterranean coast. Palaeogeogr Palaeoclimatol Palaeoecol 299:289–297 https://doi.org/10.1016/j.palaeo.2010.11.009

Durand-Delga M, Kornprobst J (1985) Carte géologique de Tanger-Al Manzla (1/50000). Notes et mémoires du service géologique du Maroc, vol 294

El Alami SO, Tinti S (1991) A preliminary evaluation of the tsunami hazards in the Moroccan coasts. *Sci*. Tsunami Haz 9:31–38

El Gharbaoui A (1981) La terre et l'homme dans la péninsule tingitane: étude sur l'homme et le milieu naturel dans le Rif Occidental, vol 15. Institut scientifique

El Messaoudi B, Ait Laâmel M, El Hou M, Bouksim H (2016) Situations des fortes houles sur les côtes atlantiques marocaines. Actes Session Plénière Académie Hassan II des Sciences & Techniques, pp 79–99

El Talibi H (2016) Evidences of tsunami deposits along the Moroccan Atlantic coast (Tanger-Asilah): methodological approch, sites analyses and hazard mitigation. Universite Abdelmalek Essaadi

El Talibi H, El Moussaoui S, Zaghloul MN, Aboumaria K, Wassmer P, Mercier JL (2016) New sedimentary and geomorphic evidence of tsunami flooding related to an older events along the Tangier-Asilah coastal plain, Morocco. Geoenvironmental Disasters 3. Springer International Publishing, 14 https://doi.org/10.1186/s40677-016-0049-6

Friedman GM, Sanders JE (1978) Principles of sedimentology. Wiley, New York

Fujiwara O, Kamataki T (2007) Identification of tsunami deposits considering the tsunami waveform: An example of subaqueous tsunami deposits in

Holocene shallow bay on southern Boso Peninsula, Central Japan. Sedimentary Geol 200:295–313 Elsevier. https://doi.org/10.1016/j.sedgeo.2007.01.009
Gigout M (1959) Ages par radiocarbone de deux formations des environs de Rabat (Maroc). C R Hebd Seances Acad Sci 249. GAUTHIER-VILLARS/EDITIONS ELSEVIER 23 RUE LINOIS, 75015 PARIS, FRANCE:2802–2803
Golberg E (1963) Geochronology with lead-210. Radioactive Dating. International Atomic Energy Agency, Vienna, pp 121–131
Gutscher MA, Baptista MA, Miranda JM (2006) The Gibraltar arc seismogenic zone (part 2): constraints on a shallow east dipping fault plane source for the 1755 Lisbon earthquake provided by modeling and seismic intensity. Tectonophysics 426:153–166 https://doi.org/10.1016/j.tecto.2006.02.024
Higman B, Bourgeois J (2008) Deposits of the 1992 Nicaragua tsunami. In: Tsunamiites. Elsevier, pp 81–103
Jaaidi, E. B., M. Ahmamou, R. Zougary, B. Chatre, B. El Moutchou, K. Malek, and K. Naim. 1993. Le littoral méditerranéen entre Tétouan et Ceuta et atlantique entre Tanger et Asilah: impact des aménagements portuaires sur la dynamique côtière. L'environnement des côtes marocaines en péril. Publ. Comité National de Géographie du Maroc, Aménagement littoral et évolution des côtes: 21–30
Kaabouben F, Baptista MA, Iben Brahim A, El Mouraouah A, Toto A (2009) On the moroccan tsunami catalogue. Nat Hazards Earth Syst Sci 9:1227–1236 https://doi.org/10.5194/nhess-9-1227-2009
Keating BH, Wanink M, Helsley CE (2008) Introduction to a tsunami-deposits database. In: Tsunamiites. Elsevier, pp 359–381
Koster B, Reicherter K (2014) Sedimentological and geophysical properties of a ca. 4000year old tsunami deposit in southern Spain. Sedimentary Geol 314:1–16 Elsevier B.V. https://doi.org/10.1016/j.sedgeo.2014.09.006
Krishnaswamy S, Lal D, Martin JM, Meybeck M (1971) Geochronology of lake sediments. Earth Planetary Sci Lett 11:407–414 Elsevier. https://doi.org/10.1016/0012-821X(71)90202-0
Lario J, Zazo C, Goy JL, Silva PG, Bardaji T, Cabero A, Dabrio CJ (2011) Holocene palaeotsunami catalogue of SW Iberia. Quaternary Int 242:196–200 Elsevier Ltd and INQUA. https://doi.org/10.1016/j.quaint.2011.01.036
Leorri E, Freitas MC, Zourarah B, Andrade C, Mellas S, Cruces A, Griboulard R, Lopes V (2010) Multiproxy approach to characterize an overwash deposit: Oualidia lagoon (Moroccan Atlantic coast). Geogaceta:7–10
Martínez Solares JM, López Arroyo A (2004) The great historical 1755 earthquake. Effects and damage in Spain. J Seismology 8:275–294 https://doi.org/10.1023/B:JOSE.0000021365.94606.03
Medina F, Mhammdi N, Chiguer A, Akil M, Jaaidi EB (2011) The Rabat and Larache boulder fields; new examples of high-energy deposits related to storms and tsunami waves in North-Western Morocco. Nat Hazard 59:725–747 Springer. https://doi.org/10.1007/s11069-011-9792-x
Mellas S (2012) Atlantique marocain Evaluation du risque tsunamique sur le littoral atlantique marocain. In: Université Paul Valéry - Montpellier 3. Université Chouaib Doukkali, El Jadida
Mhammdi N, Medina F, Belkhayat Z, El Aoula R, Geawahri MA, Chiguer A (2020) Marine storms along the Moroccan Atlantic coast: an underrated natural hazard? J Afr Earth Sci 163:103730 Elsevier B.V.https://doi.org/10.1016/j.jafrearsci.2019.103730
Mhammdi N, Medina F, Kelletat D, Ahmamou M, Aloussi L (2008) Large boulders along the Rabat coast (Morocco); possible emplacement by the November, 1st, 1755 AD tsunami. Sci Tsunami Hazard 27. Tsunami Society International: 17–30
Mhammdi N, Medina F, Trentesaux A, Font E, Belkhayat Z, Geawhari MA (2015) Sedimentary evidence of Palaeo-tsunami deposits along the Loukkos estuary (Moroccan Atlantic Coast). J Tsunami Soc Int 32:77–95
Monge Soares AM, Matos Martins JM (2010) Radiocarbon dating of marine samples from gulf of Cadiz: the reservoir effect. Quat Int 221:9–12 https://doi.org/10.1016/j.quaint.2009.10.012
Morton RA, Gelfenbaum G, Jaffe BE (2007) Physical criteria for distinguishing sandy tsunami and storm deposits using modern examples. Sediment Geol 200:184–207 https://doi.org/10.1016/j.sedgeo.2007.01.003
Nachite D, Bekkali R, Macias A, Anfuso G (2008) El estuario de Tahaddart: las bases para una gestión integrada de un espacio en plena transformación. Service de Publication de l'Université de Cadix, Espagne
Nanayama F (2008) Sedimentary characteristics and depositional processes of onshore tsunami deposits: an example of sedimentation associated with the 12 July 1993 Hokkaido–Nansei-Oki earthquake tsunami. In: Tsunamiites. Elsevier, pp 63–80
NCEI. 2020. Natural hazards data, images and education. https://ngdc.noaa.gov/hazard/hazards.shtml. Accessed July 7
Omira R, Baptista MA, Matias L, Miranda JM, Catita C, Carrilho F, Toto E (2009) Design of a sea-level tsunami detection network for the Gulf of Cadiz. Nat Hazard Earth Syst Sci 9:1327–1338 https://doi.org/10.5194/nhess-9-1327-2009
ONE (2002) Rapport d'Etude d'Impact sur l'Environnement de la Centrale à Cycles Combinés de Tahaddart, vol II. Rapport Final, Rabat, vol 186
Raji O, Dezileau L, Von Grafenstein U, Niazi S, Snoussi M, Martinez P (2015) Extreme Sea events during the last millennium in the northeast of Morocco. Nat Hazards Earth Syst Sci 15:203–211 https://doi.org/10.5194/nhess-15-203-2015
Reimer PJ, Baillie MGL, Bard E, Bayliss A, Beck JW, Blackwell PG, Ramsey CB et al (2013) IntCal13 and Marine13 radiocarbon age calibration curves 0–50,000 years cal BP. Radiocarbon 55:1869–1887 Cambridge University Press. https://doi.org/10.2458/azu_js_rc.55.16947
RGPH (2014) Recensement Général de la Population et de l'Habitat. Royaume du Maroc, Rabat
Richter TO, van der Gaast S, Koster B, Vaars A, Gieles R, de Stigter HC, De Haas H, van Weering TCE (2006) The Avaatech XRF Core scanner: technical description and applications to NE Atlantic sediments. Geol Soc Lond, Spec Publ 267:39–50 https://doi.org/10.1144/GSL.SP.2006.267.01.03
Robbins JA, Edgington DN (1975) Determination of recent sedimentation rates in Lake Michigan using Pb-210 and Cs-137. Geochimica Cosmochimica Acta 39:285–304 Elsevier. https://doi.org/10.1016/0016-7037(75)90198-2
Ruiz F, Rodríguez-Vidal J, Abad M, Cáceres LM, Carretero MI, Pozo M, Rodríguez-Llanes JM et al (2013) Sedimentological and geomorphological imprints of Holocene tsunamis in southwestern Spain: An approach to establish the recurrence period. Geomorphology 203:97–104 Elsevier B.V. https://doi.org/10.1016/j.geomorph.2013.09.008
Scileppi E, Donnelly JP (2007) Sedimentary evidence of hurricane strikes in western Long Island, New York. Geochem Geophysics Geosystems 8 John Wiley & Sons, Ltd. https://doi.org/10.1029/2006GC001463
Smith JN, Walton A (1980) Sediment accumulation rates and geochronologies measured in the Saguenay Fjord using the Pb-210 dating method. Geochimica Cosmochimica Acta 44:225–240 Elsevier. https://doi.org/10.1016/0016-7037(80)90134-9
Snoussi M, Ouchani T, Niazi S (2008) Vulnerability assessment of the impact of sea-level rise and flooding on the Moroccan coast: the case of the Mediterranean eastern zone. Estuarine Coastal Shelf Sci 77:206–213 Elsevier. https://doi.org/10.1016/j.ecss.2007.09.024
Stuiver, M, P J Reimer, and R W Reimer. 2017. CALIB 7.1 [WWW program]
Taaouati M (2012) Morphodynamique des plages et évolution su trait de côte sur le littoral atlantique du Tangerois (Maroc Nord Occidental): Approches saisaonnière et pluridécénnale par techniques de la gématique. Université Abdel Malek Essaâdi, Faculté des Sciences, Tétouan
Theilen-Willige, B., H Ait malek, M. Ait Ougougdal, E. Boumaggard, W. Bourchet, M. Chaibi, A. Charif, et al. 2013. Use of RapidEye-Data for the Detection of Natural Hazard Prone Areas (Earthquake , Tsunami , Landslides , Desertification) in W-Morocco
Tisnérat-Laborde N, Poupeau JJ, Tannau JF, Paterne M (2001) Development of a semi-automated system for routine preparation of carbonate samples. Radiocarbon 43:299–304 Cambridge University Press. https://doi.org/10.1017/S0033822200038145
Vigliotti L, Andrade C, Conceição F, Capotondi L, Gallerani A, Bellucci LG (2019) Paleomagnetic, rock magnetic and geochemical study of the 1755 tsunami deposit at Boca do Rio (Algarve, Portugal). Palaeogeography Palaeoclimatol Palaeoecol 514:550–566 Elsevier. https://doi.org/10.1016/j.palaeo.2018.10.030
Ward SN, Day S (2001) Cumbre Vieja Volcano-Potential collapse and tsunami at La Palma, Canary Islands. Geophysical Res Lett 28:3397–3400 Wiley-Blackwell. https://doi.org/10.1029/2001GL013110
Woodruff JD, Irish JL, Camargo SJ (2013) Coastal flooding by tropical cyclones and sea-level rise. Nature 504:44–52 https://doi.org/1s0.1038/nature12855

Publisher's Note

Springer Nature remains neutral with regard to jurisdictional claims in published maps and institutional affiliations.